

Supplementary

Anthropogenic Photolabile Chlorine in the Cold-Climature City of Montreal

Ryan Hall ¹, Oleg Nepotchatykh ², Evguenia Nepotchatykh ² and Parisa A. Ariya ^{1,3,*}

¹ Department of Chemistry, McGill University, 801 Sherbrooke Street West, Montréal, QC H3A 0B8, Canada; ryan.hall2@mail.mcgill.ca

² PO-Laboratories, 609 McCaffrey Street, Saint-Laurent, QC H4T 1N3, Canada; info@po-labs.com (O.N.); evguenia88@gmail.com (E.N.)

³ Department of Atmospheric and Oceanic Sciences, McGill University, 805 Sherbrooke West, Montréal, QC H3A 0B9, Canada

* Correspondence: parisa.ariya@mcgill.ca; Tel.: +(514)-398-6931 (ext. 3615)

1. Image of Cl₂-RPGE Tube



Figure S1. Image of Cl₂-RPGE tube, next to a ruler for size measurement.

2. Calibration and Validation Parameters of Cl₂-RPGE Tube–GC-MS Method

Method Linearity

Linearity of the method studied in the full range: 1 to 200 ppt of Cl₂ in helium, prepared by precise dilution.

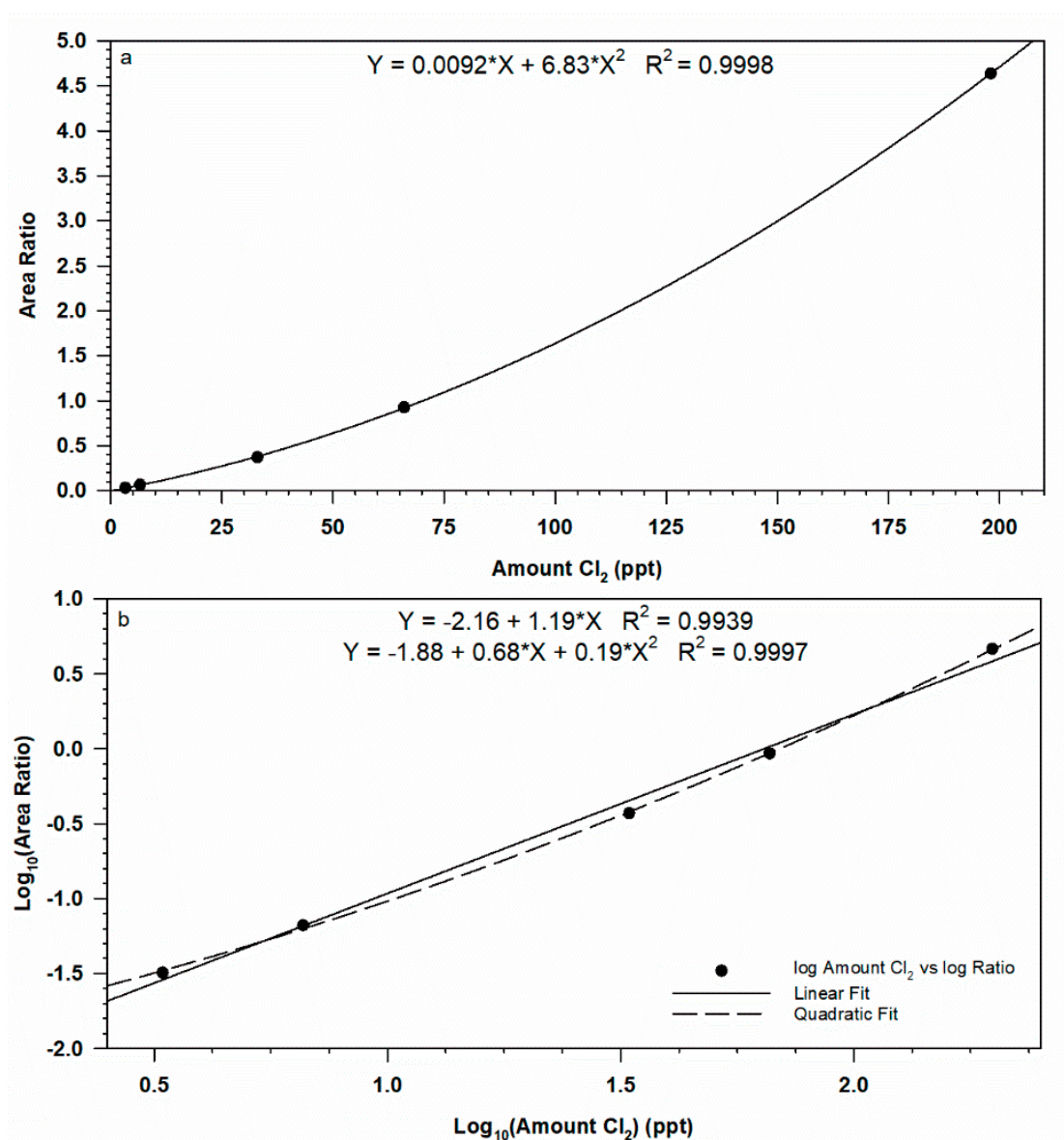


Figure S2. Representative calibration plots with (a) showing quadratic fit with raw calibration data, and (b) showing a log-log calibration plot with both linear and quadratic fits, demonstrating that a quadratic fit still fits the data best. The area ratio compares the peak area of the internal standard (naphthalene-d8) to the peak area of the measured known amount of Cl₂ (in ppt Cl₂).

Method has excellent linearity with $r^2 = 0.9998$, the calibration curve is quadratic as expected, because efficiency of ionization is proportional to the concentration of analyte molecules in the ion volume of the electron-impact MS source.

Signal to Noise (S/N), Limit of Detection (LOD) and Limit of Quantification (LOQ)

The Signal to Noise level is calculated by dividing Cl₂ 10 ppt (30 L sample) signal to the level of baseline noise. The limit of quantitation is calculated based on Signal-to-Noise of blank/low samples as $S/N = 10$. The limit of detection is calculated based on Signal-to-Noise of blank/low samples as $S/N = 3$.

Table S1. Tabulated parameters identifying the lower limits of the sampling method.

Cl ₂ Concentration (ppt)	10
Average signal (height) of 10 ppt Cl ₂	4010
Average noise	40
S/N	100.25
LOQ (ppt)	1.00
LOD (ppt)	0.30

Method Accuracy

Method accuracy was measured by spike and recovery of chlorine at medium (50 ppt) and low (5ppt) concentration:

Table S2. Method accuracy with spike and recovery of 50 ppt.

Sample	Specified Amount, ppt	Calculated Amount, ppt	Difference %
spike 50 ppt Cl ₂	50	50.0	0
spike 50 ppt Cl ₂	50	50.2	0.43
spike 50 ppt Cl ₂	50	49.9	-0.23
spike 50 ppt Cl ₂	50	51.0	2.08
spike 50 ppt Cl ₂	50	49.0	-1.97
spike 50 ppt Cl ₂	50	50.0	-2.1
		RSD%	1.43

Table S3. Method accuracy with spike and recovery of 5 ppt.

Sample	Specified Amount, ppt	Calculated Amount, ppt	Difference %
spike 5 ppt Cl ₂	5	4.96	-0.8
spike 5 ppt Cl ₂	5	5.26	5.1
spike 5 ppt Cl ₂	5	5.30	5.9
spike 5 ppt Cl ₂	5	5.26	5.2
spike 5 ppt Cl ₂	5	5.21	4.1
spike 5 ppt Cl ₂	5	5.15	2.9
		RSD%	2.24

Method Repeatability

To determine method repeatability the same gas sample mixture analyzed six times.

Table S4. Method repeatability over six 50 ppt samples.

Sample	Specified Amount, ppt	Calculated Amount, ppt	Difference %
repeatability	50	50.2	0.47
repeatability	50	51.1	2.28
repeatability	50	50.4	0.81
repeatability	50	51.1	2.15
repeatability	50	51.0	1.94
repeatability	50	52.0	3.9
		RSD%	1.11

Method Intermediate Precision

To estimate method intermediate precision 10 ppt calibration samples of chlorine in helium were prepared and analyzed during three subsequent days:

Table S5. Method intermediate precision determination day 1.

Sample	Specified Amount, ppt	Calculated Amount, ppt	Difference %
Day 1-1	10	10.1	0.50
Day 1-2	10	10.2	2.30
Day 1-3	10	10.1	0.80
Day 1-4	10	10.2	2.20
Day 1-5	10	10.2	1.90
Day 1-6	10	10.4	3.90
RSD%			1.11

Table S6. Method intermediate precision determination day 2.

Sample	Specified Amount, ppt	Calculated Amount ppt	Difference %
Day 2-1	10	9.95	-0.50
Day 2-2	10	10.3	3.20
Day 2-3	10	10.1	1.30
Day 2-4	10	9.79	-2.10
Day 2-5	10	10.2	1.60
Day 2-6	10	9.86	-1.40
RSD%			1.84

Table S7. Method intermediate precision determination day 3.

Sample	Specified Amount, ppt	Calculated Amount, ppt	Difference %
Day 3-1	10	9.93	-0.70
Day 3-2	10	9.79	-2.10
Day 3-3	10	9.31	-6.90
Day 3-4	10	10.1	1.30
Day 3-5	10	9.65	-3.60
Day 3-6	10	9.39	-6.10
RSD%			2.88

3. Simplified Setup Diagram

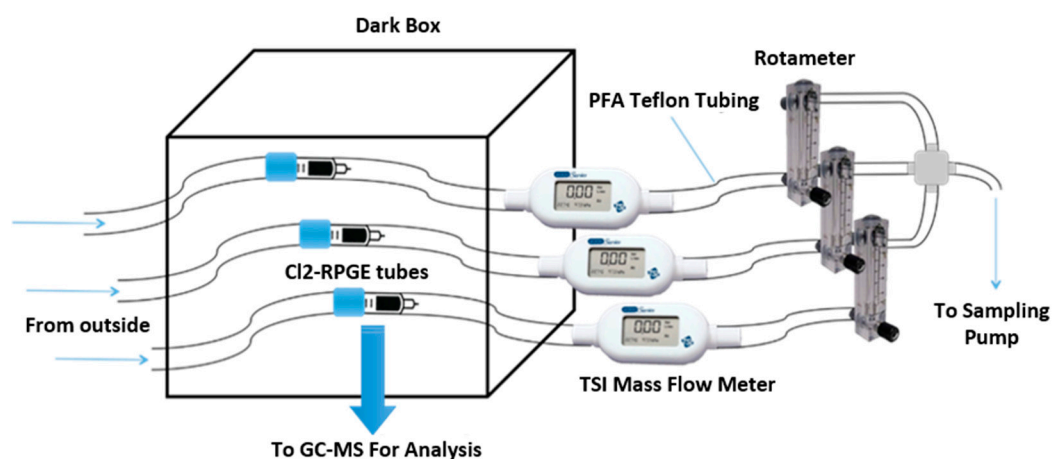


Figure S3. Simplified schematic of sampling setup for regular dark sampling. Figure shows 3 TSI mass flow meters to represent a simplified setup, when a single TSI mass flow meter was used to read flow through each line individually at various times throughout a sampling run. The dark box measures 24 in × 24 in × 24 in. Modification for UV experiments involves turning on 4 UV A lamps installed upright in each corner of the ventilated dark box, and inserting a 150 mL cylindrical Pyrex vessel between the inlet line and the Cl₂-RPGE tube.

4. Comparison of UV Lamp and Solar Radiation Wavelengths to Absorption Cross Section Wavelengths for Selected Relevant Molecules

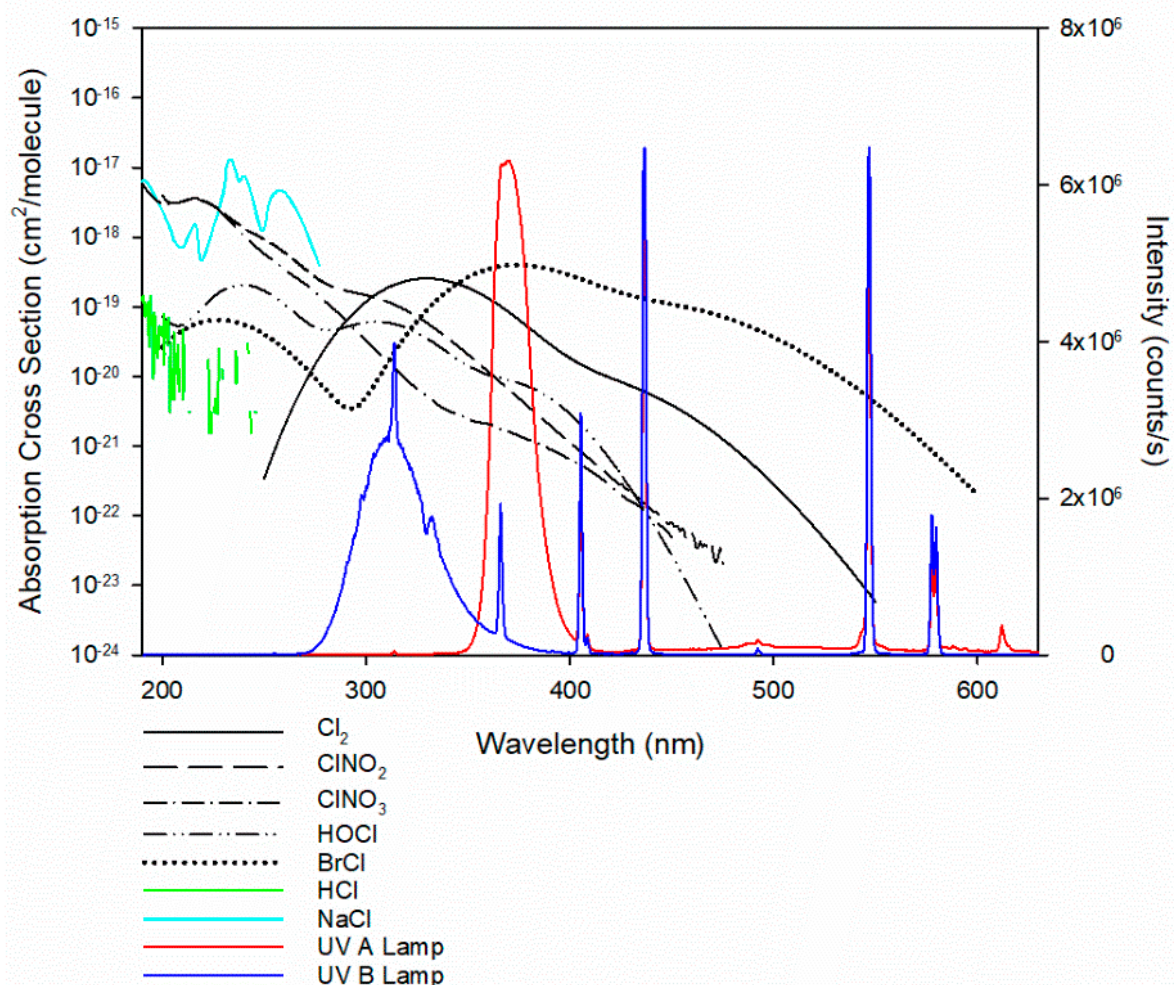


Figure S4. Comparison of UV A (red) and UV B (blue) lamp wavelengths to absorption wavelengths for relevant molecules [1]. The absorption cross sections of selected relevant gaseous chlorine containing compounds (Cl_2 [2], ClNO_2 [3], ClNO_3 [4], HOCl [5], and BrCl [6]) are shown in black. The absorption cross sections of HCl [7] and NaCl [8] are shown in green and cyan to emphasize that they are not within range of UV A or UV B wavelengths. The absorption cross section Y-axis is logarithmic in order to display all species on the same plot. The model of the UV A and UV B lamps are Hitachi F15t8/BL and Sankyo Denki GT15T8E respectively. The UV lamp spectra were collected using an Ocean Optics Jaz Spectrometer connected to an optical fiber (P100-2-UV/VIS) that was the probe directed directly at the light source. The optical fiber has a diameter of $100 \mu\text{m}$. The resulting spectra were obtained by averaging 50 scans with an integration time of 10 ms. Note that UV lamps do not generate the same exact spectra consistently, and as such direct comparison contain large amount of uncertainties.

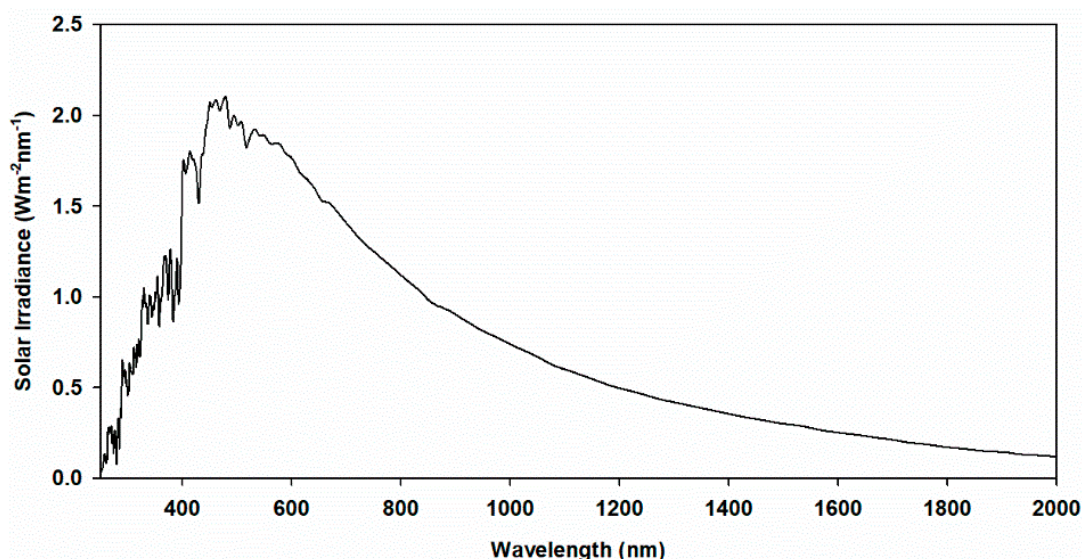


Figure S5. Plot of solar irradiance spectrum to show relevant tropospheric wavelengths [9].

5. Sources of Uncertainty

There are inherent errors associated with the sorbent method sampling procedure. The majority of sampling errors in this case are related to the flow of air through the sorbent, or in improper storage of the devices before or after loading. The devices themselves introduce a small error due to the inherent properties of their construction. The sorbent itself provides a resistance to the flow of air and, as the packing of each device cannot be perfectly identical, each Cl₂-RPGE tube provides a slightly different resistance. This property results in the flow having to be slightly adjusted for each device at the beginning of each sampling period, in order to produce equal flow through all concurrently sampling devices. Associated with this is the main component of human error during sampling, which is the manual adjustment and monitoring of airflow for each individual device. This is done by adjusting the rotameters while looking at the flow reading on the TSI mass flow meter. This error is minimized, however, due to the determined end amount of chlorine taking into account the actual flow through each device individually. Even if the flow is slightly different through each Cl₂-RPGE tube, it will be properly accounted for during analysis.

The errors associated with the transport and storage of samples is easily minimized, but if proper procedure is not followed, these errors can have large impacts on the resulting data. If the sample is exposed to light, it may result in photolysis of any chlorine containing compounds still present, but unreacted, as well as possible interaction with any particulates present in the device as well. The larger error, however, is if the sorbent material remains exposed to air for a period of time and are not in a sealed container, which is preferably filled with inert gas. If the sorbent remains exposed to open air before sampling, it will gradually become oxidized, which will impact the efficiency of the chlorination. Also, whether it is before or after the sampling period, exposure to air will result in the sorbent reacting with chlorine other than from the sampling period. Air exposure of the devices may be accounted for, for a reasonable period of exposure, by the blanks run during analysis, but it is an error that can be almost completely removed by utilizing proper storage procedures.

The last process with associated errors is the sample treatment and processing before GC-MS analysis. The amounts of acetone and naphthalene-d₈ internal standard must be as consistent as possible. We achieve this by using an Eppendorf repeater for all injected volumes, with a separate tip used for each compound to eliminate contamination. If the volume of acetone is not consistent across all samples, this will result in varying dilution factors for each sample, which will affect amounts of chlorine measured. The internal standard must also be very consistent across samples, as this is the reference by which the amount of chlorine is determined. The main source of human error during sample processing is the extraction and injection of the sample solution into the GC-MS. This is done using a gas-tight syringe, and it relies on the personnel to be consistent in amounts injected, and to

be sure to remove any bubbles from the syringe. If not done consistently, injection volumes will vary between samples, introducing random differences. Errors associated with this part of the procedure can be minimized by using an auto-sampler.

6. Time Series Plots of Cl^-/CO , O_3/CO , NO_x/CO and $\text{PM}_{2.5}/\text{CO}$ Concentration Ratios

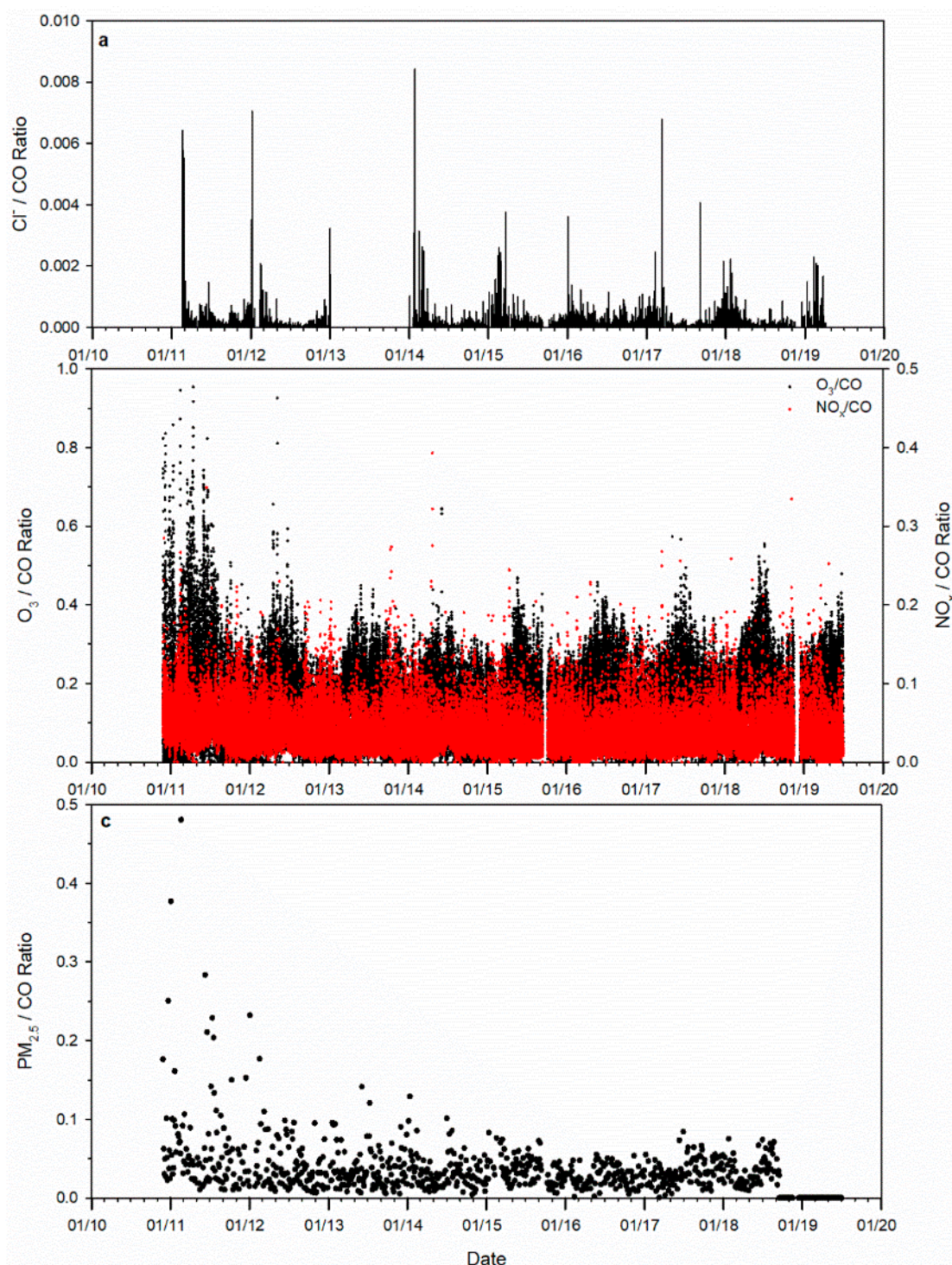


Figure S6. Time series plots of (a) Cl^-/CO , (b) O_3/CO and NO_x/CO , and (c) $\text{PM}_{2.5}/\text{CO}$ concentration ratios to show possible impact of boundary layer height on measurements and trends.

7. Time Series Plot of O₃ and NO_x Product Concentrations

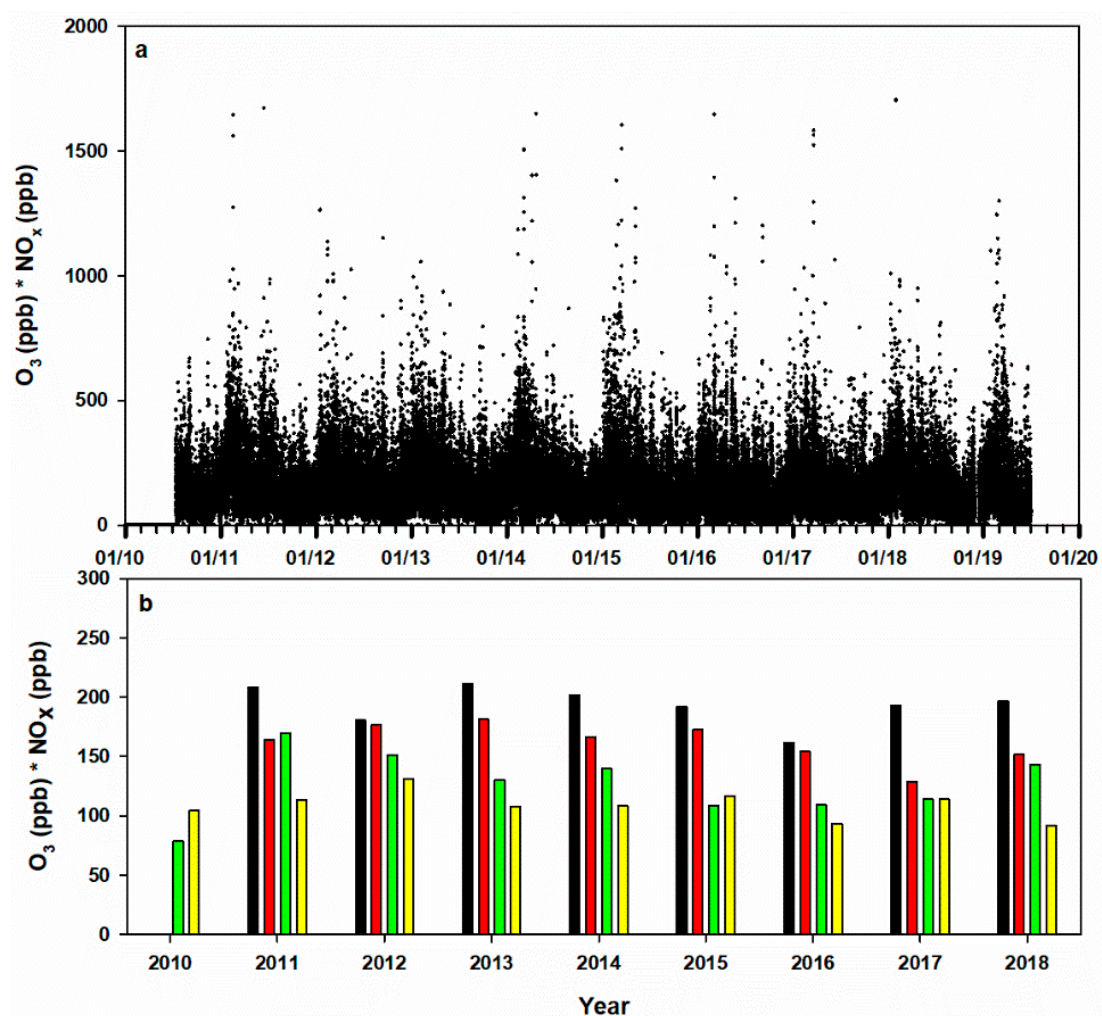


Figure S7. Time series of O₃ and NO_x product concentrations as (a) validated data and (b) seasonal averages to demonstrate the seasonality, and to support the predicted increase of ClNO₂ in winter.

8. Time Series Plot of O₃ and NO_x Product Concentrations Divided by CO

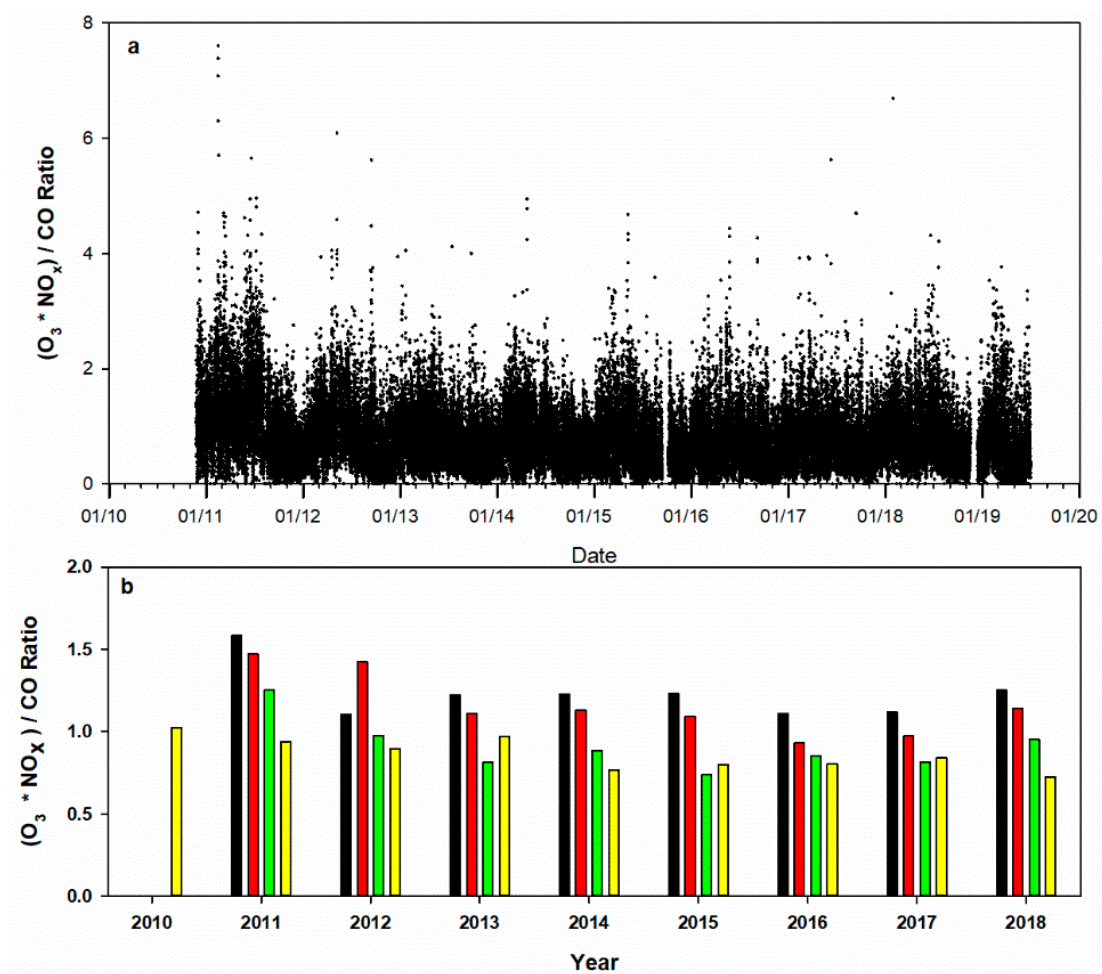


Figure S8. Time series of O₃ and NO_x concentration product divided by CO concentration as (a) validated data and (b) seasonal averages to demonstrate the seasonality. Division by CO is to show possible impact of boundary layer height on measurements and trends.

9. Representative Chromatograms

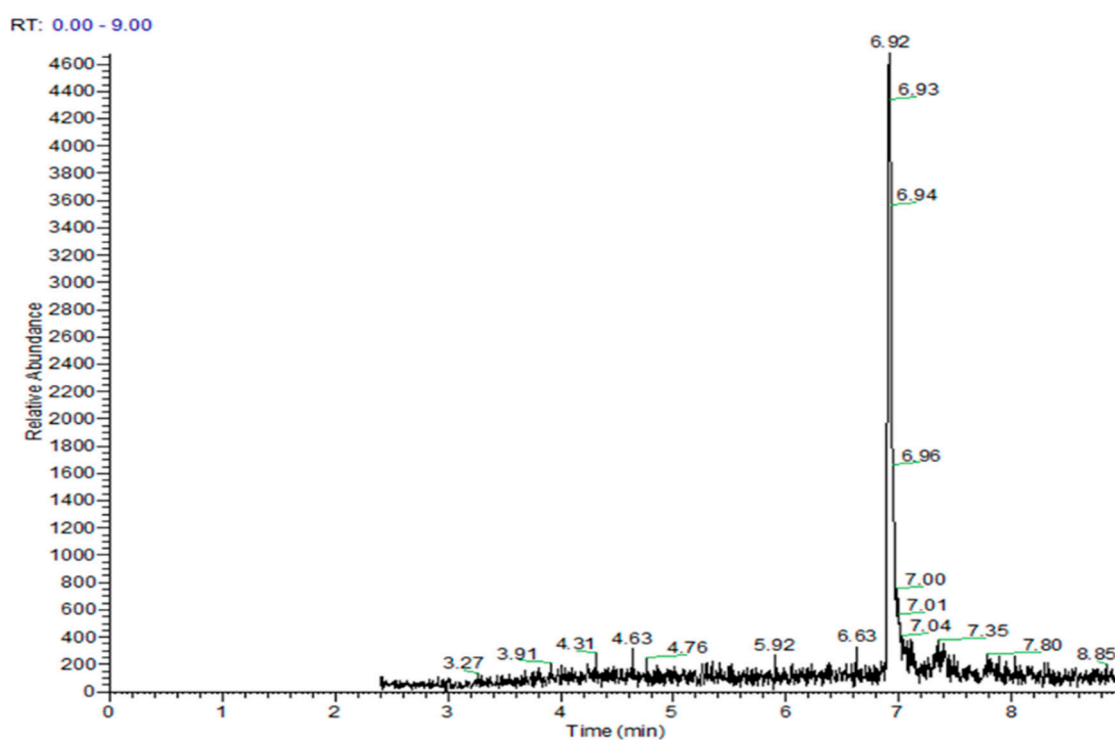


Figure S9. Representative SIM chromatogram showing detection of the chlorinated product with $m/z = 178$ from a loaded Cl₂-RPGE tube used for a calibration standard. Peak of interest is at 6.92 min, and corresponds to a value of 76 ng/m³ of chlorine standard.

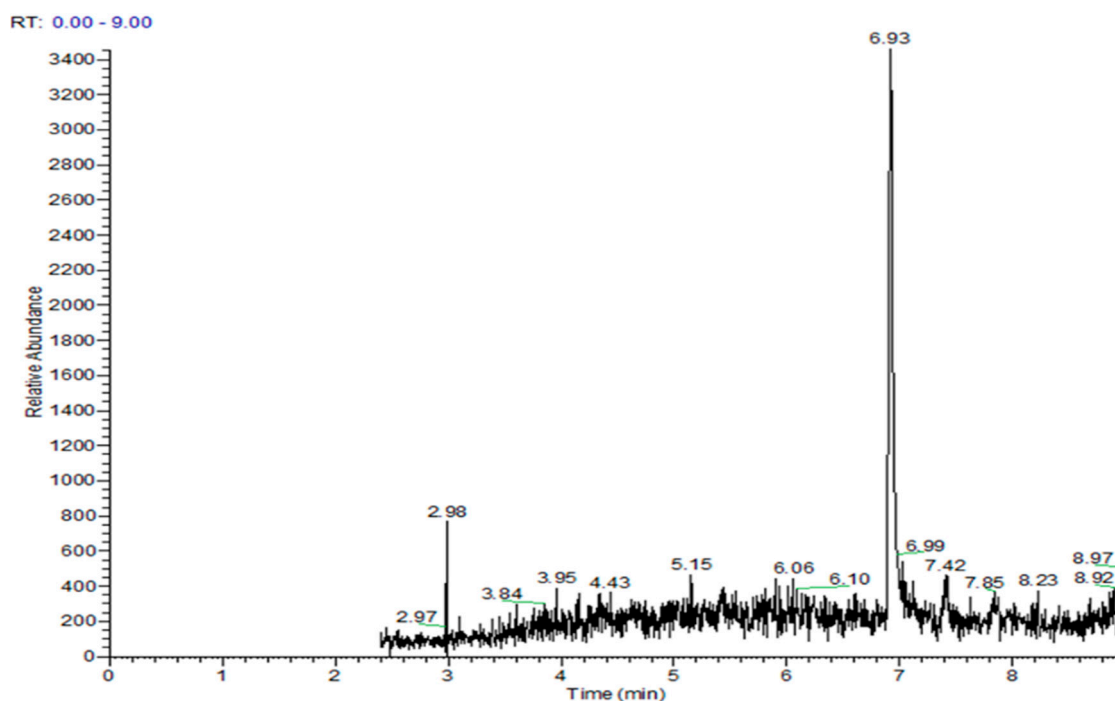


Figure S10. Representative SIM chromatogram showing detection of the chlorinated product with $m/z = 178$ from a loaded Cl₂-RPGE tube used for ambient sampling on 3 April 2019. Peak of interest is at 6.93 min.

References

1. Keller-Rudek, H.; Moortgat, G.K.; Sander, R.; Sørensen, R. The MPI-Mainz UV/VIS spectral atlas of gaseous molecules of atmospheric interest. *Earth Syst. Sci. Data* **2013**, *5*, 365–373. doi:10.5194/essd-5-365-2013.
2. Maric, D.; Burrows, J.P.; Meller, R.; Moortgat, G.K. A study of the UV-visible absorption of molecular chlorine. *J. Photochem. Photobiol. A Chem.* **1993**, *703*, 205–214. doi:10.1016/1010-6030(93)85045-A.
3. Ghosh, B.; Papanastasiou, D.K.; Talukdar, R.K.; Roberts, J.M.; Burkholder, J.B. Nitryl chloride (ClNO₂): UV/Vis absorption spectrum between 210 and 296 K and O(³P) quantum yield at 193 and 248 nm. *J. Phys. Chem. A* **2012**, *116*, 5796–5805. doi:10.1021/jp207389y.
4. Molina, L.T.; Molina, M.J. Chlorine nitrate ultraviolet absorption spectrum at stratospheric temperatures. *J. Photochem.* **1979**, *11*, 139–144. doi:10.1016/0047-2670(79)80047-7.
5. Barnes, R.J.; Sinha, A.; Michelsen, H.A. Assessing the contribution of the lowest triplet state to the near-UV absorption spectrum of HOCl. *J. Phys. Chem. A* **1998**, *102*, 8855–8859. doi:10.1021/jp9835869.
6. Maric, D.; Burrows, J.P.; Moortgat, G.K. A study of the UV-visible absorption spectra of Br₂ and BrCl. *J. Photochem. Photobiol. A Chem.* **1994**, *83*, 179–192. doi:10.1016/1010-6030(94)03823-6.
7. Brion, C.E.; Dyck, M.; Cooper, G. Absolute photoabsorption cross-sections (oscillator strengths) for valence and inner shell excitations in hydrogen chloride, hydrogen bromide, and hydrogen iodide. *J. Elec. Spec. Rel. Phen.* **2005**, *144–147*, 127–130. doi:10.1016/j.elspec.2005.01.010.
8. Silver, J.A.; Worsnop, D.R.; Freedman, A.; Kolb, C.E. Absolute photodissociation cross sections of gas phase sodium chloride at room temperature. *J. Chem. Phys.* **1986**, *84*, 4378. doi:10.1063/1.450060.
9. Harder, J. SORCE SIM Level 3 Solar Spectral Irradiance Daily Means V026, Greenbelt, MD, USA, Goddard Earth Sciences Data and Information Services Center (GES DISC). doi:10.5067/IGSTXAANZ79N.



© 2020 by the authors. Submitted for possible open access publication under the terms and conditions of the Creative Commons Attribution (CC BY) license (<http://creativecommons.org/licenses/by/4.0/>).